Raman Spectroscopy: a tool for examining isotopic exchange rate; researching influences on $^{16}O/^{18}O$ exchange between bicarbonate and water.

Menno Euwes 6025054
Master Thesis
Utrecht, June 2023

Abstract

Our understanding of the paleoclimate record heavily relies on the $^{18}O/^{16}O$ ratio of oceanic water recorded in calcium carbonates. This record depends on the balance of the $^{18}O/^{16}O$-ratio between $H_2O(l)$ and the Dissolved Inorganic Carbon (DIC) system. Studying the exchange and factors that can impact this balance can improve our understanding of the $^{18}O/^{16}O$ ratio and therefore the climate record. In this study, Raman Spectroscopy is used to investigate the exchange of oxygen isotopes between $H_2{}^{18}O(l)$ and $HCO_3^-(aq)$ on a minute scale, building on the findings of Geisler et al. (2012) who demonstrated the use of Raman Spectroscopy for monitoring a similar sort of exchange for $CO_3^{2-}(aq)$.

The oxygen isotopic exchange rate is determined by the change from ^{16}O to ^{18}O in bicarbonate over time. The inclusion of ^{18}O was determined by the change in shift of the bicarbonate peak (CO-H stretch) between natural levels of the ^{18}O-isotope in the bicarbonate and the 48% ^{18}O in bicarbonate as the $H_2{}^{18}O(l)$ and $HCO_3^-(aq)$ balanced out. This led to an increase of 1% ^{18}O to bicarbonate being equivalent to a decrease in Raman shift of 2.04 cm^{-1}. It was therefore possible to calculate the oxygen isotopic exchange rate per minute.

This method was used to study the effect of pH value and ionic strength on the oxygen isotopic exchange rates of various salt solutions. Which, the pH value had a strong correlation to the oxygen isotopic exchange rate, and the ionic strength did not show a correlation. The pH value determines the relative activity of the different DIC species, controlling the amount of the activity of $CO_2(aq)$ in the solution. The $CO_2(aq)$ is needed for the exchange of oxygen between $H_2O(l)$ and $HCO_3^-(aq)$ via the hydration and hydroxylation reactions determining the overall oxygen isotope exchange rate.

Next to that, the change of the bicarbonate band was investigated with increasing different levels of ^{18}O. The change in the shape of the band was determined to be a result of the formation of the individual bands of the four isotopologues due to the increased levels of ^{18}O which overlapped each other forming a broader envelope. A model was created to determine the location of these isotopologues. Next to that, the Full Width Half Maximum was studied, which showed no correlation to the oxygen isotopic exchange rate of ^{18}O in bicarbonate.

This research showed Raman Spectroscopy as a powerful tool for investigating real-time exchange for oxygen isotopes between $H_2O(l)$ and $HCO_3^-(aq)$. The exchange rates that were found had a strong correlation to the pH value of the solution, whilst the ionic strength showed no correlation. The Full Width Half Maximum was too variable to find a correlation to the oxygen isotopic exchange rate. It is important to study the effect of pH on the precipitation rate of calcium carbonate and its rate and compare it to the oxygen exchange rate to see if this can improve our understanding of the $^{18}O/^{16}O$ ratio.

Introduction

The kinetics and mechanisms of oxygen isotope exchange between water and dissolved inorganic carbon (DIC) are factors that contribute to oxygen compositions observed in carbonate minerals (Devriendt et al., 2017; Gabitov et al., 2012; Guo et al., 2019; Kim et al., 2014; Tarutani et al., 1969). Studying the processes controlling isotope exchange will lead to improvement of the interpretations of $^{18}O/^{16}O$ variation in minerals. However, new methods are necessary to monitor isotope exchange in DIC species. In this regard, Raman Spectroscopy is investigated as a new tool to monitor isotope exchange rates of ^{18}O into aqueous HCO_3^-. This innovative method has the potential to improve our understanding of the kinetics of isotope exchange and mechanisms in the H_2O-carbonate system.

The trends of $^{18}O/^{16}O$ are used to interpret the paleotemperature of seawater. The reconstructions are constrained by clumped isotope thermometry and the equilibrium carbonate water fractionation factor based on slow calcite precipitation (Kim et al., 2007). In their theory, an assumption is made that the dissolution-precipitation process of the carbonate is slow enough to facilitate the balancing of oxygen isotope exchange to reach equilibrium. However, there is currently no convincing evidence that this is the case for natural systems. Also, the influence of dissolved salts on the exchange of oxygen isotopes may result in potential effects on the isotopic composition (Guo et al., 2019). Therefore, it is essential to understand the impact of different dissolved salts and their concentration on the kinetics of the oxygen isotope exchange process of the carbonate.

The rate of oxygen isotope exchange is not only based on the equilibrium fractionation of oxy-anions and the precipitating mineral at a given temperature but also on the various ion species. These species can affect the isotopic fractionation of the oxygen atoms in the dissolution/precipitation system of minerals. For example, it has been found that the outer rims of calcite crystals contain a lower $^{18}O/^{16}O$ ratio content than the inner crystals due to dissolution reprecipitation processes, which only affect the outside of the crystal (Tarutani et al., 1969). The solution in which the carbonate dissolves differ from the levels of the DIC and δO^{18} in which the carbonate was precipitated. The dissolved carbonate ions will balance out to the DIC of its surroundings and subsequently equal the $^{18}O/^{16}O$ ratio levels of the $H_2O(l)$ as the isotopes are exchanged within the DIC pool.

Raman spectroscopy is a valuable non-destructive technique which can chemically analyse solutions, among other samples. The technique uses a monochromatic incident light to interact with the vibrational modes of molecular groups. After the interaction, some of the photons gain or lose some of their energy compared to the original wavelength of the incident light, resulting in a change in their wavelength. Raman Spectroscopy examines this shift in photon wavelength, with the incident light wavelength set to 0, mainly focusing on photons losing energy after the interaction, called Stokes scattering. At room temperature, this form of Raman scattering forms bands of higher intensity compared to Anti-stokes scattering which creates better Raman graphs (King & Geisler, 2018). The amount of Stokes scattering depends on bond strength, the mass of the vibrating atoms, point groups, as well as short- and long-range symmetry. The dependency on the atom's weight makes Raman Spectroscopy a useful technique to analyse isotopologues, especially the lighter isotopes as they have a higher difference in isotopic weights over their heavier counterparts.

Raman spectroscopy is a valuable tool for the analysis of DIC species in the H_2O-carbonate system ($CO_2(aq)$, $H_2CO_3(aq)$, $HCO_3^-(aq)$ and $CO_3^{-2}(aq)$). The Raman band of $HCO_3^-(aq)$ has been established in previous research (Bonales et al., 2013; Geisler et al., 2012; Rudolph et al., 2007), but the effect of ^{18}O exchange between $H_2O(l)$ to $HCO_3^-(aq)$ on the Raman graph remains unclear. In a similar study, Geisler et al. (2012) used a Raman Spectroscope to monitor the real-time exchange of oxygen isotopes between CO_3^{2-} and H_2O, demonstrating that the effect of the additional weight of ^{18}O over ^{16}O affects

Raman scattering enough to create new bands for the individual isotopologues in the Raman graph. This allowed for tracking the ^{18}O distribution and determination of the isotopic exchange rate. The same methodology is applied to investigate the usefulness of the ^{18}O exchange between the H_2O-HCO_3^- system.

Following the previous work of Geisler et al. (2012) this current research will answer some remaining questions regarding the ability to use Raman Spectrometry for studying oxygen isotope exchange rates.

This research aims to answer the following questions:

- Can Raman Spectroscopy be used to determine the exchange rate $^{16}O/^{18}O$ isotopes between $H_2O(l)$ and $HCO_3^-(aq)$?
- How do different salt ions, differences in ionic strength and pH influence the exchange rates?
- How does the Full With Half Maximums (FWHM) of the C-O band compare in the presence of different ions?
- Can the different peaks of the HCO_3^- isotopologues be located and quantified in the Raman Spectrum?

1.1 Dissolved Inorganic Carbon and ^{18}O exchange.

Dissolved Inorganic Carbon (DIC) is an umbrella term for the four different carbonate species CO_2(aq), CO_3^{2-}(aq), HCO_3^-(aq), and H_2CO_3(aq). The last, true carbonic acid is noted as part of CO_2(aq) because they are both neutrally charged, and chemically inseparable, and H_2CO_3 only contributes ~0.3% towards the total dissolved CO_2 (Zeebe & Wolf-Gladrow, 2001). The relative distribution of the DIC is described by the following relationships (Beck et al., 2005; Lueker et al., 2000; Zeebe, 2001).

$$CO_2(g) \leftrightarrow CO_2(aq) \quad (1)$$

$$CO_2(aq) + H_2O\ (l) \leftrightarrow H_2CO_3(aq)\ \leftrightarrow HCO_3^-(aq) + H^+(aq) \quad (2)$$

$$CO_2(aq) + \ OH^-\ (aq) \leftrightarrow HCO_3^-(aq) \quad (3)$$

$$HCO_3^-(aq) \leftrightarrow CO_3^{2-}(aq) + H^+(aq) \quad (4)$$

The relative distribution of the different carbonates is determined by the equilibrium constants of the previous reactions. The transfer of oxygen takes place via hydration (2) and/or hydroxylation (3) of CO_2(aq) depending on the pH of the solution (Beck et al., 2005; Devriendt et al., 2017; Uchikawa et al., 2021). This means, that the concentration of CO_2(aq) determines the pace of the oxygen transferred from water to carbon dioxide. To reach ^{18}O-enriched CO_2, true carbonic acid is degassed according to $H_2C^{16}O_2{}^{18}O$(aq) => $C^{16}O^{18}O$(aq) + $H_2{}^{16}O$(l). This ^{18}O-enriched CO_2(aq) returns to reactions (2) and (3) creating all forms of $HC^{16}O_n{}^{18}O_{[3-n]}$ from which the $C^{16}O_3{}^{18}O_{(3-n)}$ can form (Geisler et al., 2012).

1.1.1 Isotopic equilibrium between aqueous species

To understand the isotopic exchange between $H_2O(l)$ and DIC, it is key to understand how the oxygen isotopic equilibrium is attained. Isotopic equilibrium refers to the state where the isotopic exchange between the aqueous species and water has reached a balance. Both chemical and isotopic equilibria work the similar manner in terms of drive to reach their respective equilibria. While the chemical distribution of the DIC species in solution is attained within seconds, reaching an oxygen isotopic equilibrium can take hours to days to form (Devriendt et al., 2017). This means that isotopes between the different species are not at equilibrium, despite the chemical distribution being reached. The relatively slow isotopic exchange rate occurs primarily via the hydration (2) and hydroxylation (3) of $CO_2(aq)$ for the carbonate species as this is the fastest way to exchange oxygen isotopes from ^{18}O-water into carbonate DIC species as the dissolved ion species all contain 3 oxygen molecules (Beck et al., 2005; Devriendt et al., 2017; Zeebe & Wolf-Gladrow, 2001). This rate is determined by the availability of $CO_2(aq)$ in a system, which depends on the pH of the system (see section 1.2) (Beck et al., 2005). The presence of the enzyme Carbonic Anhydrase (CA) also influences the isotopic exchange rate as it catalyses the inter-conversion of $CO_2(aq)$ and $HCO_3^-(aq)$ through CO_2 hydration ant its reverse reaction, which is the primary pathway for direct oxygen exchange between DIC species and $H_2O(l)$. The presence of CA reduces the time needed for ^{18}O equilibration (Uchikawa & Zeebe, 2012).

The fastest way to get oxygen molecules incorporated in anions appears to be via a reaction. For carbonate species this is via reaction of $CO_2(aq)$ and $H_2O(l)$ to $H_2CO_3(aq)$ which includes an oxygen molecule into the carbonate species. This is also true for other anions species such and aqueous phosphate. In the work of O'Neil et al. (2003) the incorporation of oxygen atoms is discussed in two ways; the main way is the equivalent of true carbonic acid route in which the hydrolysis of the P-O-P bond reacts with $H_2O(l)$ forming two groups P-OH and HO-P of which one of the oxygen atoms comes from water. The alternative mechanism is based on the research of Bunton et al. (1961) in which it is proposed that H-bonded activated complexes allow the separation of the OH bond from the P atom, and reformation of the P-OH bonds, therefore promoting oxygen exchange between water and phosphate via reformation. The alternative version does not happen as the faster way is the incorporation of oxygen atoms into anions via a reaction.

1.1.2 Isotope fractionation.

One of the key processes in the field of stable isotopes is isotope fractionation. Isotopes of the same element can have different chemical and/or physical properties in atoms and molecules, these differences are called isotope effects. Isotope effects can cause isotope fractionation among the different substances, such as an unequal distribution or are unequal partitioned among the different substances. One example in which isotopic effects can cause isotopic fractionation is the partitioning between reactants and products of a chemical reaction (Zeebe & Wolf-Gladrow, 2001).

Among the different forms of isotopic fractionation there are two types that are relevant to this study.

- Equilibrium fractionation occurs when different compounds or phases are in thermodynamic equilibrium. So if there is no net change in the backward and forward change in chemical reactions, different molecular species containt different ratios of isotopes due to fractionation (Zeebe & Wolf-Gladrow, 2001).

- Kinetic fractionation occurs during incomplete or uni-directional reactions. This form of fractionation happens when the reaction rates between different isopotes are different. In Zeebe & Wolf-Gladrow (2001) an example is consider for the hydration of CO_2(aq) as a unidirectional reaction: $CO_2(aq)+H_2O \rightarrow HCO_3^-(aq)+H^+(aq)$. In this case the lighter isotope ^{12}C prefers to be in the HCO_3^-(aq) at a higher rate than its heavier form ^{13}C. Therefore, the HCO_3^-(aq) will be enriched in ^{12}C whilst the CO_2(aq) will be enriched in ^{13}C, due to its isotope effects.

In the work of Geisler et al. (2012) it has been noted that these effects play a role in the reactions, but the Raman Spectroscope is unable to detect these processes. This is because the Raman Spectroscope can only detect changes on percent scale whilst these processes are on permille scale. It is important to know that during isotopic exchange rates isotopic fractionation occurs but for this research at a too low rate to detect.

1.2 Influence of pH value.

The fact that either H^+ or OH^- is participating in the reactions (1 to 4) indicates that the pH plays a role in the relative distribution of the DIC species (Fig. 1). Additionally, both carbonate and bicarbonate have alkaline properties, which enable them to neutralise acids in the solution (Michałowski et al., 2012). The addition of $NaHCO_3$ can change the pH of a solution significantly enough to alter the balance of DIC (reactions 1 to 4). The pH versus activity is shown in the Bjerrum plot (Fig. 1), which has been calculated for conditions of 25 °C and 1 atmosphere. Next to pH, parameters like temperature, pCO_2, and salinity also affect the distribution (Yuen et al., 2016).

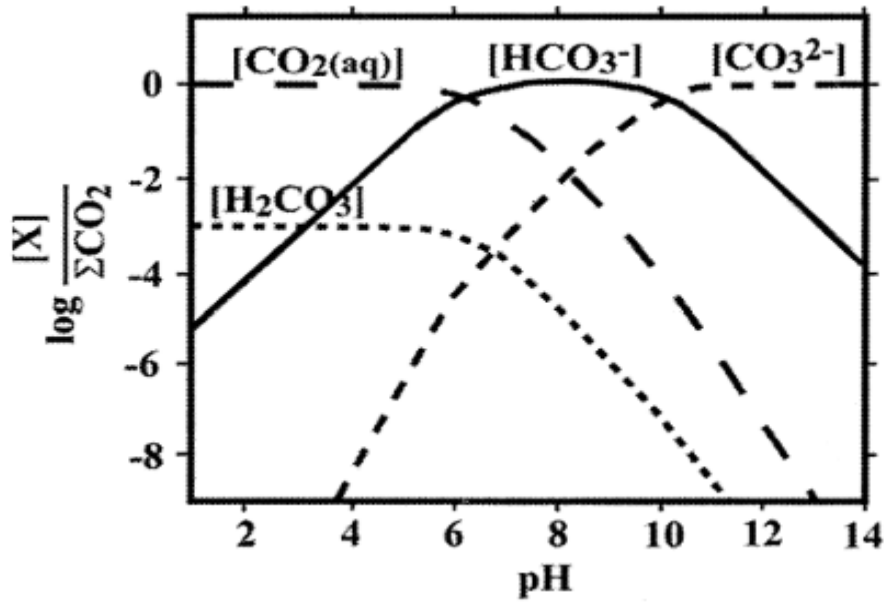

Figure 1: Bjerrum diagram at 1 atrm and 25 °C (Beck et al., 2005) in a closed system showing the relative proportion of activity of DIC species over the total DIC at different pH values. The ΣCO_2 stands for the total sum of all the DIC species.

1.3 The effect of ionic strength.

Dissolved salts can affect the oxygen isotope exchange, as the oxygen isotope salt effect. This effect is believed to exist as water molecules form a hydration sphere around the aqueous ions. The water molecules which are concentrated in this hydration sphere preferably are made up of the heavier atoms, whilst the lighter molecules sit in the broken-structure region. The balance between these hydration regions is a factor in determining the isotopic exchange regime between the water of the hydration sphere and the remaining bulk solution. For example, the addition of Ca^{2+}(aq) leads to the bulk water being depleted of ^{18}O and the hydration shell being enriched in ^{18}O (Guo et al., 2019).

The effect of these hydration shells is less apparent in the oxygen exchange rates found in DIC species. As in the study of Beck et al. (2005), three experiments were conducted with $NaHCO_3$ solutions at high pH (>11). This high pH was chosen to keep $[CO_3^{2-}(aq)]+[NaCO_3^{-}(aq)]$ above 93% of the total amount of DIC, with three adjustments in which the $NaCO_3^-$ was ~18%, 26%, and 45% of the total DIC. These experiments indicated that the effect of weak ion pairs is negligible in the DIC-H_2O fractionation factors. It is worth noting that these experiments were conducted at high pH, and the effect may differ at other pH values, but this is one of the few studies conducted on this topic.

In the study of Kim et al. (2014), experiments were conducted on a Na-Cl-CO_2-H_2O system (at pH ~7.9 and ~10.6). Their study found that the effect of ionic strength on oxygen isotope fractionation in carbonate and bicarbonate pairs is negligible. However, their study examined the final fractionation rates and did not study the effects of ionic strength during the entire fractionation. The effects of ionic strength on the oxygen isotope exchange rates for the DIC systems during its fractionation remains unknown.

1.4 Raman Spectroscopy.

The Raman spectrometer uses molecular vibrations to provide information about chemical structures and physical forms. This data is obtained by identifying characteristic spectral patterns, and it can also be used to (semi-) quantitatively determine the amount of a substance. One advantage of this method is that it can be used on solids, liquids, or gases. Another advantage is that it can examine aqueous solutions in situ within a container (Wiley & Edwards, 2005). Modern techniques are mainly non-destructive and can analyse up to a few nanometres in size. An important factor for this study is that Raman spectroscopy can detect changes in isotopic composition (King & Geisler, 2018).

The Raman spectrometer consists of a light source, monochromator, sample holder, and detector. When monochromatic light (also called incident light) interacts with a molecule, it results in light scattering. This scattering is created when a photon interacts with molecular vibrations, their combined excited states create a virtual energy level for an infinitesimally short period. When this virtual state is then de-excited, a photon is released containing the same, higher, or lower energy level than the incident light (Cialla-May et al., 2019).

There are two main types of light scattering, Rayleigh scattering and Raman scattering. Rayleigh scattering, also known as elastic scattering, is very common. it occurs when a photon maintains the same wavelength from before and after the interaction with a molecule ($\nu_s=\nu_i$). Whilst the photons can change direction after the interaction, they keep the same wavelength. Most light is scattered as Rayleigh scattering and does not provide useful information.

In contrast, Raman scattering is an inelastic scattering process that occurs when light interacts with molecules, this results in a shift in wavelength of the scattered photons compared to the incident photons. The interaction between the incident photons and a molecule causes a (de)activation in the molecular vibration, which results in the release of a scattered photon with a higher or lower wavelength compared to that of the incident light. The shifting photons can be described by two types of Raman scattering: Stokes and anti-Stokes scattering. Stokes scattering occurs when the interaction of the photon and the molecule lead to an increase in the wavelength of the scattered photon, resulting in a higher wavelength. Anti-Stokes scattering happens when the scattered photon decreases in wavelength (Das & Agrawal, 2011).

The Raman Spectrometer uses the principles of inelastic light scattering to provide an analysis of the chemical structures and physical forms of samples. The Raman shift, which is the difference in wavelength of the scattered light [λ_s] and the incident light [λ_i] ([cm^{-1}], x-axis). The wavelength of incident light is typically set at 0 in a Raman spectrum. In the Raman spectrum, the intensity of the Raman scattering (y-axis) is plotted against the Raman shift (x-axis). The shift is calculated using the formula: $\Delta\nu = \left(\frac{1}{\lambda_i(nm)} - \frac{1}{\lambda_s(nm)}\right)\frac{(10^7 nm)}{(cm)}$.

The Raman Spectroscopy is generally focussed on the Stokes scattering, as the bands are more evident at room temperature than Anti-Stokes scattering. The change in energy of the scattered light depends on the required energy of the oscillation of the atoms around their equilibrium position. This means that the intensity of each molecular group depends on bond strength, the mass of the vibrating atoms, site symmetry within a structure, and short- and long-range symmetry. Therefore, every molecular group contains multiple internal modes: twisting, stretching, and bending. These motions are generated by a specific amount of energy, resulting in multiple bands on the Raman spectrum specific to molecular groups, giving all molecular groups a unique fingerprint (King & Geisler, 2018).

The masses of the atoms in molecular groups are one of the influencing factors for the location and shape of the associated Raman band. The use of Raman spectroscopy enables different isotopologues to be identified. The same molecular structure can show unique spectra for the different isotopic compositions. For instance, Geisler (2018) demonstrated that the different ^{18}O isotopologues for carbonate showed unique peaks for different isotopic compositions (see Fig. 2). The heights of the individual bands can also be used to quantify the distribution of the overall isotopologues in percentages (Geisler et al., 2012).

In contrast, introducing ^{18}O isotopes in chromium oxide resulted in the shift and broadening of a single peak (880 cm^{-1}) for Cr-O-Cr vibrations of polychromate species (Weckhuysen & Wachs, 1997). This broadening is due to the formation of new peaks around the same wavelength. The new bands overlap with each other, leading to the widening of the overall band.

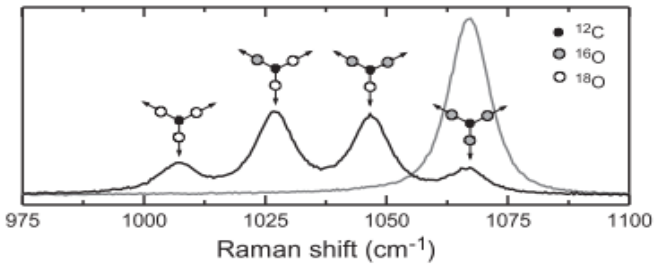

Figure 2: The change from natural carbonates (grey line) to the equilibrium of the 48% enriched carbonates (black line). (Geisler et al. 2018)

1.5 Research on ^{18}O Exchange between water and carbonate.

Although no research has been done on the real-time exchange rates of ^{18}O between water and bicarbonates using Raman Spectroscopy, Geisler et al. (2012) have performed similar research on carbonates. Despite having different chemical properties, both carbonate and bicarbonate have four similar isotopologues related to ^{18}O, $HC^{16}O_n{}^{18}O_{(3-n)}{}^-$ and $C^{16}O_n{}^{18}O_{(3-n)}{}^{2-}$ with n [=1,2,3] referring to the amount of ^{18}O included.

At the start of their experiments (see Fig. 3), Geisler et al. (2012) observed a single large peak at 1067 cm^{-1}, which indicates the peak of bicarbonate in an unadulterated setting, containing ~0.2% ^{18}O. Following the exchange of ^{18}O, four new peaks appear, one for every ^{18}O isotopologue (Fig. 3). This result demonstrates that the Raman Spectroscopy can be used to monitor the ^{18}O exchange from $H_2{}^{18}O$ to $C^{16}O_3$.

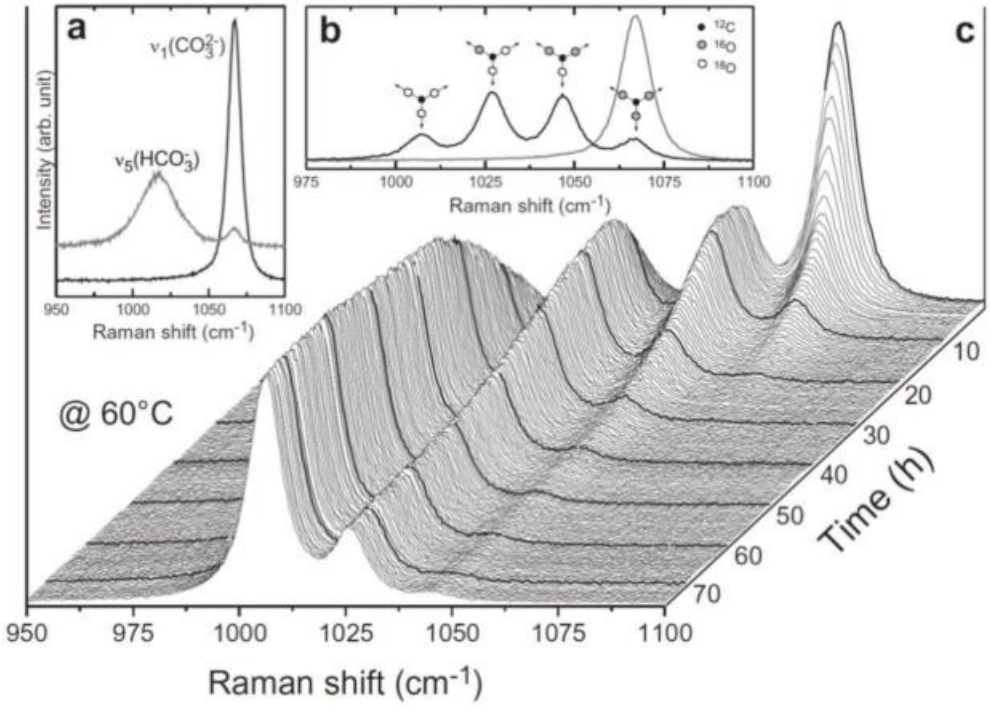

Figure 3: a) Raman shift of a solution of 1 M $NaHCO_3$ (grey line) and 1 M Na_2CO_3 (black line) from the rand of 950 to 1100 Raman shift (cm^{-1}). The $\nu_1(CO_3^{2-})$ band at 1067 cm^{-1} and the ν_5 band at 1017 cm^{-1}. The CO_3^{2-} band is found in the 1M $NaHCO_3$, while the HCO_3^- band is not found at 1017 cm^{-1} in the 1M Na_2CO_3. b) Solution of 1 M Na_2HCO_3 solution mixed with $H_2{}^{18}O$. The grey line was collected immediately after mixing, and the black line after 10 hours. In the black line, 3 new bands (for the other 3 isotopologues) have formed at lower frequencies and the original band went down quite a lot. c) A waterfall plot over time of 1 M Na2CO3 (~97% H218O) up to 75 hours at 60 °C. Showing the relative increase and decrease of the different isotopologues over time with the H218O water. From (Geisler et al., 2012)

Methods

2.1 Conducting the experiments.

The experiment aims to track the kinetics of oxygen atoms between water and bicarbonates depending on ionic strength, and pH value. This is done by tracing the exchange rate between the ^{18}O water to $H^{16}CO_n{}^{18}O_{(n-1)}$.

The bulk solutions for the individual experiments were prepared the day before the experiment, the specific compositions for each experiment are given in Table 1. The error of weighing was kept within a margin of ±0.1 g of the given weights on a scale measuring three digits beyond the decimal place. Following the initial weighing, 10 ml of UHQ water was added, and measured with a graduated cylinder. The mixture of salts and water was thoroughly shaken and left to settle overnight to ensure that the salts were completely dissolved. The ion concentrations (table 2) were replicated in 10 mL solutions to measure their pH values and ionic strengths.

Table 1: The preparation for the different experiments prepared in 200 µl vials. The 0.80 MgCl2 was determined via PHREECQ to be of equivalent ionic strength of that of 0.5 M NaCl based on the formed ion pairs. Note: the experiments are referred to according to this table, the first number corresponds to the experiment number and the second number indicates the replicate number.

Solution	1	2	3.0	3.05	3.1	4	Final experimental solution	
Concentration	1.00 M $NaHCO_3$	98% $H_2{}^{18}O$	UHQ water	1.00 M NaCl	2.00 M NaCl	0.80 M $MgCl_2$		
Experiment #	Amount of each solution (µL)						Ion concentration	Isotope enrichment
1	50	100	50	-	-	-	0.25 M $NaHCO_3$	49% ^{18}O
2	100	100				-	0.50 $NaHCO_3$	49% ^{18}O
3	50	100	-	50	-	-	0.25 M $NaHCO_3$ 0.50 M NaCl	49% ^{18}O
4	50	100	-	-	50	-	0.25 M $NaHCO_3$ 1.00 M NaCl	49% ^{18}O
5	50	100	-	-	-	50	0.25 M $NaHCO_3$ 0.20 M $MgCl_2$	49% ^{18}O
6	50	100	25	-	-	25	0.25 M $NaHCO_3$ 0.10 M $MgCl_2$	49% ^{18}O

The experiments were conducted with a *WITec Alpha 300* Raman spectrometer, which was equipped with a 488 nm laser and 600 grooves/mm grating. The spectrometer was fitted on the 10X Zeiss EC Epiplan-Neofluar Disc 10x/0.25 objective lens, and the spectral centrum was set to 2250 cm^{-1}. The experimental parameters were set using the program *WITec Control Five,* and the data were analysed in *WITec Project Five* software. The spectrometer was set to acquire 25 data points, with each data point consisting of five accumulations with an integration time of 60 seconds.

The experiments aimed to investigate the exchange rates of ^{18}O isotopes between ^{18}O water and bicarbonate for the first 125 minutes in the different solutions. A final solution was prepared in a 200 µl vial using a 20-200 µl pipette. The mixing procedure was executed according to the solutions in Table 1, with the first step addition of the UHQ water, $MgCl_2$ or NaCl solutions, followed by the addition of the $NaHCO_3$ solution and ending with 98% $H_2{}^{18}O$. This was done to minimize the time between the start of the ^{18}O exchange with the solution and the start of data gathering in the Raman Spectroscope. After the preparation, the vials were quickly capped, and positioned under the Raman

spectrometer. The individual experiments were done in duplicate, and those with significant variability were conducted three times. The experiments are indicated according to the numbers in Table 1, in which the called Exp. 1-1 is experiment 1 replica number 1.

2.2 Data processing.

2.2.1 Processing the input.

The raw data files that came out of the *control FIVE*, each contained multiple graphs (t=0, to t=24). the first step was to scan each graph on the impact of cosmic rays. This phenomenon does occur naturally and randomly and results in sharp spikes in graphs which are non-related to the experiment. These outliers were easily removed with *Cosmic Ray Removal (CCR)* tool. The next step was applying *background subtraction* to set the baselines to 0 for the different data sets, so the peaks could be compared better to each other. In the *background subtraction* menu, the *constant* function was used to flat parts of the individual graph to get an average height of the baseline, which was subtracted to get an average of 0.

Next, the H_2O peak around 1640 cm^{-1} was identified and its height was normalised to 1. This transformation was carried out with the *Max peak to 1* function under the *normalize* tab in the *background subtraction* menu. This was done to ensure consistency in the height of all peaks among the different data sets. This normalisation was based on the experiments having the same amount of H_2O. As a result, the H_2O peak in all data sets should have had the same height, and the ratios should have been the same compared to this peak, allowing for a more accurate and higher resolution comparisons the different graphs.

The next step was using the *fitting tool* with *PsgVoigt1* over the bicarbonate peak found at 1017 cm^{-1}. This function fits a peak underneath analysing the data. A new text file is created containing the location of the peak (x0), and the Full Width Half Maximum (FWHM) of the peak. These are used in later analysis of the data.

2.2.2 Calculating the isotopic exchange rate.

Many different parameters influence the position of the shift from the starting measurements to the end of the measurement. Therefore, logarithmic transformations of the datasets were used to describe the different measurements. These transformations compensate for the different timings between the mixing and the start of the measurements. And are taken from the study of Geisler et al. (2012).

The complete oxygen isotope exchange between the HCO_3^- and H_2O is described as:

$$HC^{16}O_3^- + 3H_2{}^{18}O \leftrightharpoons HC^{18}O_3^- + 3H_2{}^{16}O \quad (5)$$

This reaction is described using the beginning and endmember as there are different isotopologues between these steps ($HC^{18}O^{16}O_2^-$ and $HC^{18}O_2{}^{16}O^-$). To describe the presented exchange rates validly as a first-order rate expression, formula (6) from the paper in Geisler is used as it is assumed to be accurate for isotope exchange rates.

$$-\ln\big(1 - F(t)\big) = r * \frac{3[HCO_3^-] + [H_2^{18}O]}{3[HCO_3^-][H_2^{18}O]} * t = r * \left(\frac{1}{3[HCO_3^-]} + \frac{1}{[H_2^{18}O]}\right) * t = Rt \quad (6)$$

Where R (in s^{-1}) represents the overall rate of oxygen exchange between aqueous CO_3^{2-} and H_2O, and *r* (mol L^{-1} s^{-1}) represents the overall rate accounting for the dependence of measured rate on the initial concentration of the reactants, as previously established. The assumption is made that at the end, $r_f/r_r \approx 1$, meaning that no fractionation occurs. This assumption is since fractionation is typically at concentrations below the detection limit of the Raman spectrometer system. The constant 3 accounts for the number of O atoms in CO_3^{2-}, and F(t) Is the fraction of exchanged atoms at time *t,* defined as:

$$F(t) = \frac{f_{in} - f(t)}{f_{in} - f_{eq}} \quad (7)$$

In this case, f_{in} represents the initial mole fraction (at t=0) of ^{18}O in carbonate, which would be 0.2% in natural carbonates (Geisler et al., 2012). f_{eq} is the fraction at isotopic equilibrium (t=∞) which would become <49%, as it is half of the <98% ^{18}O water that has been added, for consistency 49 is used in the calculation.

f(t) is the fraction at a certain time. It is assumed that every Raman shift (s^{-1}) is equivalent to a particular gain in fraction ^{18}O in the carbonates. The total shift is calculated by offsetting the peak between non-isotopically doped ^{18}O water (f=0,2%) and after ^{18}O water stabilised with the carbonates (f=48%).

$$f(cm^{-1}) = \frac{f_{in} - f_{eq}}{x_{in} - x_{eq}} \quad (8)$$

f(cm^{-1}) is the amount of gained fraction for each shift of 1 cm^{-1}; x_{in} and x_{eq} are the positions of the initial and equilibrium peak on the Raman graph, respectively in cm^{-1}. This has not been previously reported in other literature. *f*(t) is now calculated by comparing the change in shift over time and multiplying it by the change in fraction with each shift.

$$f(t) = (x_{in} - x_t) * f(cm^{-1}) \quad (9)$$

Finally, the data is plotted in Microsoft Excel, the STDEV.P function is used over the -ln(1-F(t)) to calculate the standard deviation.

2.2.3. Isotopic equilibrium

The overall band envelope is the sum of all the individual bands of the HCO_3^-(aq) isotopologues when these different bands have reached their respective isotopic equilibrium the band envelope stops changing shift and shape. This implies that the isotopic equilibrium (f_{eq}) has been reached when the band does not change over time anymore.

Results

3.1 Conditions of the experiment.

Each set of experiments had different pH values and ionic strengths, as the addition of different salts affected these parameters (table 2). The pH values decreased from experiment 1 to experiment 6. The expected ionic strength (I) values are predetermined using the formula $I = \frac{1}{2}\sum_{i=1}^{n} c_i {z_i}^2$, where 1/2 is included to account for both cations and anions, c_i represents the concentration of each ion in solution (mol/L), z_i represents the charge of each ion, and Σ represents the sum of all ions in solution.

No precipitation was directly observed in the 200µl vials, but after some days some of the vials showed small amounts of precipitate (Table 2).

Table 2: The pH and ionic strength values for the different experiments, and if there was any precipitation found.

Solution	Experiment #	pH	Expected Ionic Strength (M)	Ionic strength (M)	Precipitation
0.25 M $NaHCO_3$	1	8.70	0.25	0.2596	No
0.50 M $NaHCO_3$	2	8.22	0.50	0.4671	No
0.50 M NaCl + 0.25 M $NaHCO_3$	3	8.05	0.75	0.7358	No
1.00 M NaCl + 0.25 M $NaHCO_3$	4	7.96	1.25	1.2680	No
0.10 $MgCl_2$ + 0.25 M $NaHCO_3$	5	7.81	0.35	0.3029	Yes
0.20 $MgCl_2$ + 0.25 M $NaHCO_3$	6	7.58	0.63	0.6943	Yes

3.2 Identifying Raman Peaks.

The graph in Fig. 4 represents a Raman graph for 0.50 M $NaHCO_3$ without the addition of $H_2{}^{18}O$. The graphs show several bands, beginning with the prominent band between ~2900 and ~3700 cm^{-1}. This band has its main peak at ~3400 cm^{-1} and a shoulder at ~3250 cm^{-1}. The shape and locations are consistent with the findings of Kananenka & Skinner (2018), who, using an identical approach, detected a peak at 3400 cm^{-1} for the fundamental O-H stretching (ν) and a shoulder at 3250 cm^{-1} for the H-O-H bending overtone mode (2δ), which confirms the peak to have been liquid H_2O.

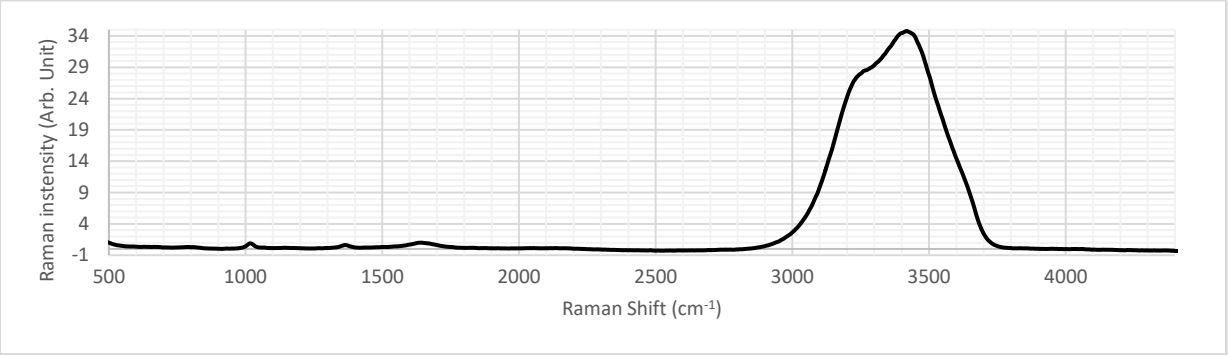

Figure 4: Analysis of 0.5 M $NaHCO_3$; 1 data point this one spectrum represents 5 accumulated spectra of 60 seconds. The data is normalised to the 1640 cm^{-1} peak and taken at room temperature and 1 atm pressure.

To further investigate the bands observed in Fig. 4, a zoomed-in snapshot (Fig. 5) has been created, which focuses on the bands with an intensity range between 0.0 and 1.2 between the Raman shift of 900 to 1900. This allows for a more detailed inspection of the observed bands.

The first band observed in the Raman spectrum is located at 1019 cm^{-1}, and with a minor shoulder at 1070 cm^{-1}. The peak corresponds to the C-OH stretch of bicarbonate, from which the peak is generally found around 1018 cm^{-1} (Bonales et al., 2013; Geisler et al., 2012; King & Geisler, 2018; Rudolph et al., 2007). This peak is used to examine the oxygen isotopic exchange. The small shoulder in the spectrum agrees with peaks found around 1067 cm^{-1}, which have been linked to the symmetric stretching vibration of carbonate [$\nu_1(CO_3)$] (Geisler et al., 2012; Rudolph et al., 2007).

The peak at 1367 cm^{-1} may correspond to either the bicarbonate band for $\nu_s CO_2$ (~1370 cm^{-1}) reported on by Cui et al. (2021) and Rudolph et al. (2007), or antisymmetric stretch of the carbonate band found at 1385 cm^{-1} (Rudolph et al., 2007). This ambiguity will be elaborated on in the discussion. The last peak at 1640 cm^{-1} agrees with the ν_2 H-O-H bending motion of liquid water (Bonales et al., 2013; Geisler et al., 2012; Kananenka & Skinner, 2018; King et al., 2011; Rudolph et al., 2007).

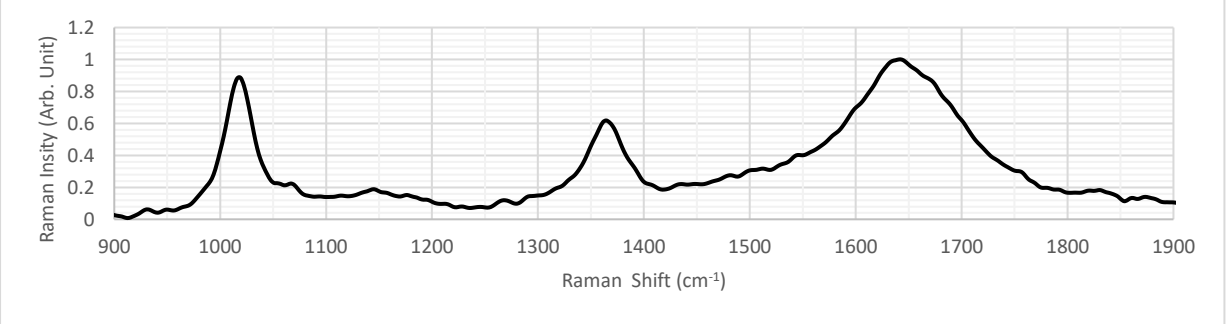

Figure 5: Analysis of 0.5 M $NaHCO_3$; zoom in on the width 900 to 1900 cm^{-1}; normalised to the peak of 1640 cm^{-1}, measured at room temperature and 1 atm pressure.

3.3 The calculation of the oxygen isotopic exchange rate.

To calculate the oxygen isotopic exchange rate of $H_2O(l)$ and $HCO_3^-(aq)$, the outer limits of the process had to be defined. These limits are the initial peak (x_{in}) and the peak when ^{18}O is in equilibrium (x_{eq}). x_i was determined at 1019.03 cm^{-1} and corresponds to the peak for bicarbonate with naturally occurring levels of ^{18}O in bicarbonate. The initial fraction (f_{in}) of ^{18}O in HCO_3^- for x_{in} is estimated to be equal to the natural levels of ^{18}O, which is 0.2%.

x_{eq} was determined at 995.52 cm^{-1} and corresponds to the peak observed after the <98% ^{18}O water and $HCO_3^-(aq)$ have reached a fully equilibrated to a fraction (f_{eq}) at 48% ^{18}O in $HCO_3^-(aq)$ (Jacobs, unpublished). These peaks (x_{in}- f_{eq}) are -23.51 cm^{-1} apart from each other, resulting in a total difference of 48% ^{18}O in the $HCO_3(aq)$.

Assuming that the shift of the peak is linear with isotopic enrichment, which is also considered for other systems such as silica (King et al., 2011), we can use the observed shift of bicarbonate to estimate the fraction of ^{18}O in HCO_3^-. Specifically, a 1cm^{-1} decrease in shift is equivalent to a 2.09% increase of ^{18}O in $HCO_3^-(aq)$.

Finally, when the amount of shift is measured against time, we find the oxygen isotopic exchange rate. For example, if 1 cm^{-1} in 10 minutes occurs, the exchange rate of ^{18}O in HCO_3^- (aq) would be 0.209%/min.

3.4 Raman analysis of a $H_2{}^{18}O$ and 0.25 M HCO_3^- solution.

In the Raman analysis of a $H_2{}^{18}O$ and 0.25 M HCO_3^- solution, points (P) were used instead of time (t). Whereas t represents a certain point in time, P represents the mean of five one-minute-long accumulations. So, P=0 is the average of the first five minutes and P=1 is the average of the interval between minutes 5-10, P=5 is the average of the solution between minutes 25-30 etc. This approach gives a more accurate and representative depiction of the data points. For the rates, the average change between the 5 minutes is still considered reliable enough to calculate rates to be in min^{-1}.

The Raman graph of the 0.25 M $NaHCO_3^-$ showed at P=0 the peak at 1016.81 cm^{-1} (Fig. 6a). Notably, the location of this peak does not coincide with x_{in}. The increments of the shift between successive points are never greater than 1.0 cm^{-1}, and the size of the increment decreases as P increases (Fig. 6b). The amplitude began at 1.19 at P=0 (table 3) going to 0.90 at P=1, after which the decline slowed, stabilising at 0.57 after P=14.

The rate of broadening for the FWHM decreases at a slower rate with the increase of P (Table 3). This becomes evident when comparing the difference between P=4 and P=9, with an increase of 4.71, to the difference between P=9 and P=14, which only increases by 1.47. These trends are consistent for all experiments. The decrease in amplitude slows and decreases more slowly over time and stabilises an amplitude of 0.57, whilst the FWHM broadens at slower rates with increasing P. Apart from the bicarbonate band, the bicarbonate band at 1060 cm^{-1} decreases from 0.26 at P=0 to 0.09 at P=24, and next to that a new band forms at ~1050 cm^{-1}.

Table 3: Results of interaction between 0.25 M NaHCO3 + 48% H218O over time. P is the nth measurement in the series. Peak position and FWHM were calculated according to the PsdVoigt1 function in fitting within PROJECT FIVE.

Measurement (P)	Position peak (cm^{-1})	FWHM (cm^{-1})	Amplitude (Rel. count to 1640 cm^{-1})
0	1016.81	31.08	1.19
1	1016.72	32.45	0.90
2	1016.27	34.56	0.74
4	1015.47	34.06	0.68
9	1013.53	38.77	0.61
14	1011.45	40.24	0.57
19	1009.94	41.22	0.57
24	1008.09	44.52	0.56

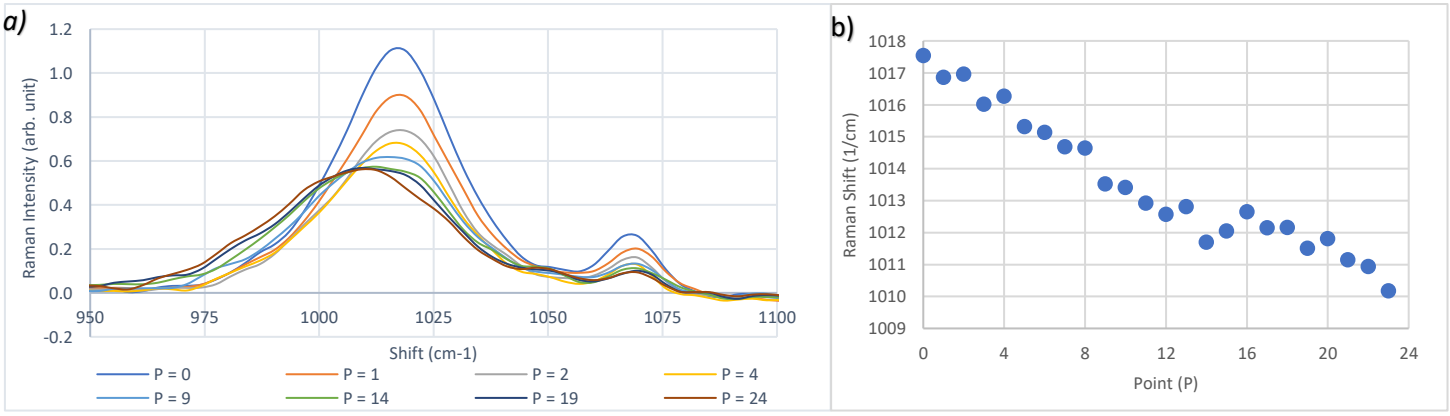

Figure 6: a) Exp-1-1 -- 0.25 M $NaHCO_3$ reacting with <98% $H_2{}^{18}O$. The different lines represent different points in time (P). This graph correlates with the table given above. b) The location of the peak (cm^{-1}) for each P

3.5 Comparison of the peak shifting rates (cm^{-1}).

The bicarbonate peak (cm^{-1}) shifting rate over the measurement (P) is a non-linear function (Fig. 7). The rates of the shift of both Exp. 1-1 (0.25 M $NaHCO_3$) and Exp. 6-1 (0.2 M $MgCl_2$ + 0.25 M $NaHCO_3$) were compared and their shifting rates declined over time. However, Exp. 1-1 had a lower rate with a less apparent concave profile compared to Exp. 6-1. Both experiments were fitted with x a third-order polynomial trendline, which both resulted in an R^2>0.95, indicating high goodness of fit. Additionally, the experiments have a different starting point (P=0), with Exp. 1-1 starting at 1017.54 cm^{-1} and Exp. 6-1 starting at 1018.50 cm^{-1}.

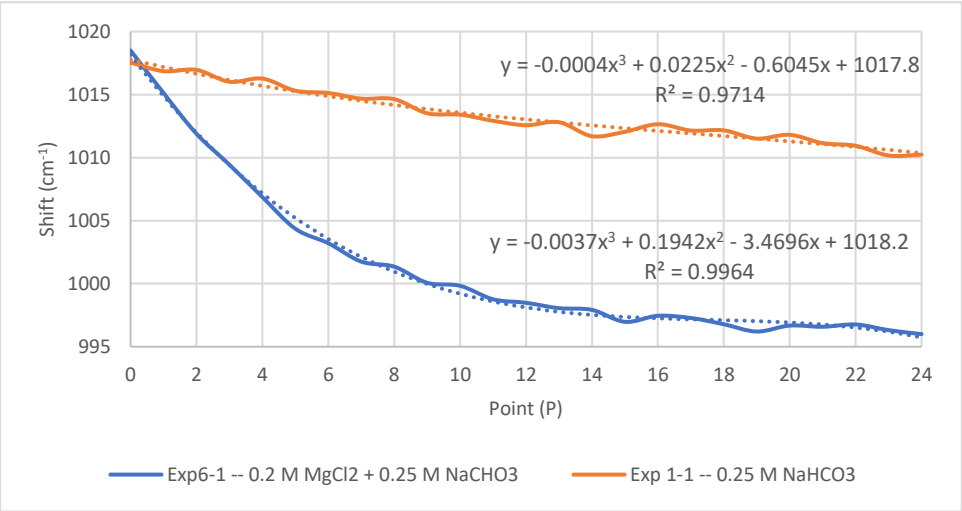

Figure 7: Output of location of the peak (cm-1) versus measurements (P). The location of the peak of each P was found in the Project FIVE software after using the PsdVoigt 1 function.

3.6 Comparing the duplicate -ln(1-F(t)) rates of 0.25 M $NaHCO_3$ solution.

By transforming the Peak Shifting rate into a -ln(1-F(t)) function, as described in section 2.2.2, the relationship between -ln(1-F(t)) and P becomes linear, providing a better comparison between the overall rates. This transformation changes the rates to go from cm^{-1}/min to fraction/cm^{-1}. Overall, these changes improve the readability and analysis of the oxygen isotopic exchange rate and the percentage of ^{18}O into HCO_3^-.

Figure 8 shows the oxygen isotopic exchange rates of Exp. 1-1 and Exp. 1-2, which were conducted at a pH of 8.7 and ionic strength of 0.2596. The blue and orange lines represent duplicate experiments conducted with a 0.25 M $NaHCO_3$ ion concentration. The slope of the trendline represents the overall rate of the exchange reaction between HCO_3^- and H_2O over time. The slopes of all three trendlines all have an R^2 value over 0.95, indicating a high degree of precision in the exchange rate measurements. The error bars represent the standard deviation. Notably, the trendlines stay within the error margin of the standard deviation, suggesting that there is no significant deviation between them.

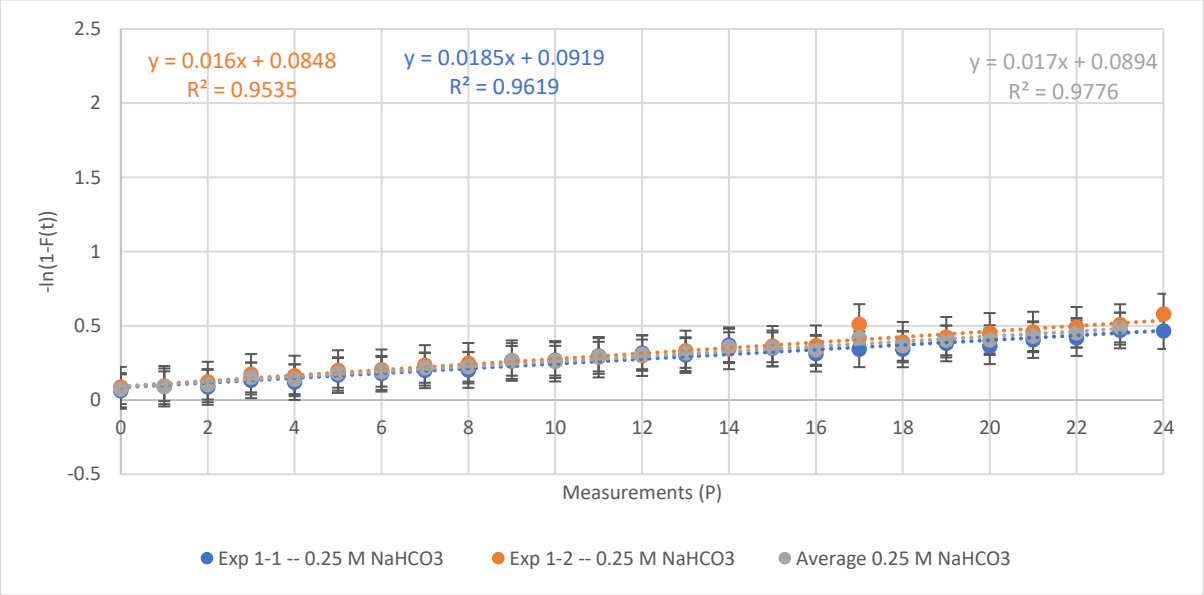

Figure 8: 0.25 M $NaHCO_3$. The isotopic exchange rates of ^{18}O into the bicarbonate ion; the logarithmic function of the fraction of exchanged oxygen molecules -ln(1-F(t)) vs measured point (P); [thus not in min^{-1}]. The orange and blue lines represent the duplicated experiment. The grey line represents the average of the 0.25 M $NaHCO_3$ experiments.

3.7 The overall oxygen isotopic exchange rates of all experiments.

Table 4 presents the oxygen isotopic exchange rates for all the experiments, which show a general trend of increasing overall rates of the exchange with the increase of the number of the experiment, except for Exp. 4-1, Exp. 4-2 and Exp. 4-3 which have lower rates compared to those of Exp. 3-1 and Exp. 3-2. Notably, Exp. 4-3 show comparable rates to the ones found for the 0.25 M $NaHCO_3$ solutions. The overall trend of increasing exchange rates is consistent with those found for the decrease in pH (Table 2). However, this correlation cannot be linked to the ionic strength as it is variable in the different experiments.

Table 4: Containing the overall rates of the oxygen isotope exchange reaction for the individual measurements, given in rates are given min^{-1}.

Experiment	Rate (min^{-1})		Rate (min^{-1})		Rate (min^{-1})	
0.25 M $NaHCO_3$	Exp. 1-1	0.0032	Exp. 1-2	0.0037		
0.50 M $NaHCO_3$	Exp. 2-1	0.0042	Exp. 2-2	0.0053		
0.50 M NaCl + 0.25 M $NaHCO_3$	Exp. 3-1	0.0087	Exp. 3-2	0.0053		
1.00 M NaCl + 0.25 M $NaHCO_3$	Exp. 4-1	0.0073	Exp. 4-2	0.0045	Exp 4-3	0.0035
0.10 M $MgCl_2$ + 0.25 M $NaHCO_3$	Exp. 5-1	0.0141	Exp. 5-2	0.0103		
0.20 M $MgCl_2$ + 0.25 M $NaHCO_3$	Exp. 6-1	0.0145	Exp. 6-2	0.0294		

3.8 Correlating the ionic strength and isotopic exchange rates.

Figure 9 shows the ionic strength (M) against the overall rates of isotopic exchange (min^{-1}). The graph indicates no correlation between the factors. For instance, Exp. 4, which has an ionic strength of 1.2680 M, exhibits a similar overall exchange rate of around 0.0035 to Exp. 1, which has an ionic strength of 0.2596 M. On the other hand, experiments 6 and 3 have comparable ionic strengths of 0.6943 M and 0.7358 M respectively, but their isotopic exchange rate differs significantly. Specifically, the rates for Exp. 6-1 0.0294 min^{-1} and Exp. 6-2 and 0.0145 min^{-1} are far apart from those of Exp. 3-1 0.0087 min^{-1} and Exp. 3-2 0.0053 min^{-1}.

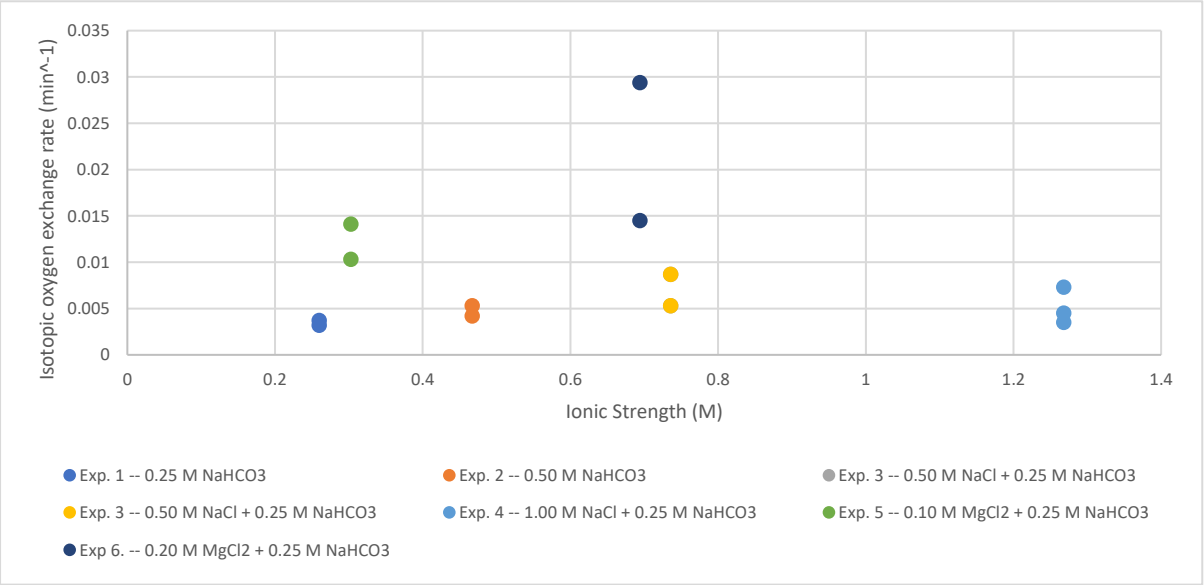

Figure 9: This figure represents the Isotopic oxygen exchange rate vs ionic strength; each colour represents a duplicate experiment.

3.9 The correlation between the pH and isotopic exchange rates.

Figure 10 shows the relationship between pH and the overall rates of the exchange reaction (min^{-1}). The graph shows a general trend of decreasing exchange rate with increasing pH. This does not apply to the NaCl experiments, in Exp. 3 shows a higher exchange rate at lower pH values than Exp. 4. (0.0053 min^{-1} for Exp. 3-1 and 0.0087 min^{-1} for Exp. 3-2, both at a pH of 8.05, versus 0.0073 min^{-1} for Exp. 4-1; 0.0045 min^{-1} for Exp. 4-2 and0.0035 min^{-1} for Exp. 4-3, all at a pH of 7.96)

Additionally, it is worth noting that the overall reaction exchange rate is slower at higher pH values and faster than for lower pH values. For example, between Exp. 1 and Exp. 2, which had a pH difference of 0.48, the isotopic exchange rate increased by 0.0013 min^{-1} (when taking the averages of the experiments). However, between Exp. 5 and Exp. 6, which had a smaller pH difference of 0.22, the average isotopic exchange increased by 0.0098 min^{-1}. This suggests that the relationship between pH and the overall isotopic exchange rate is non-linear.

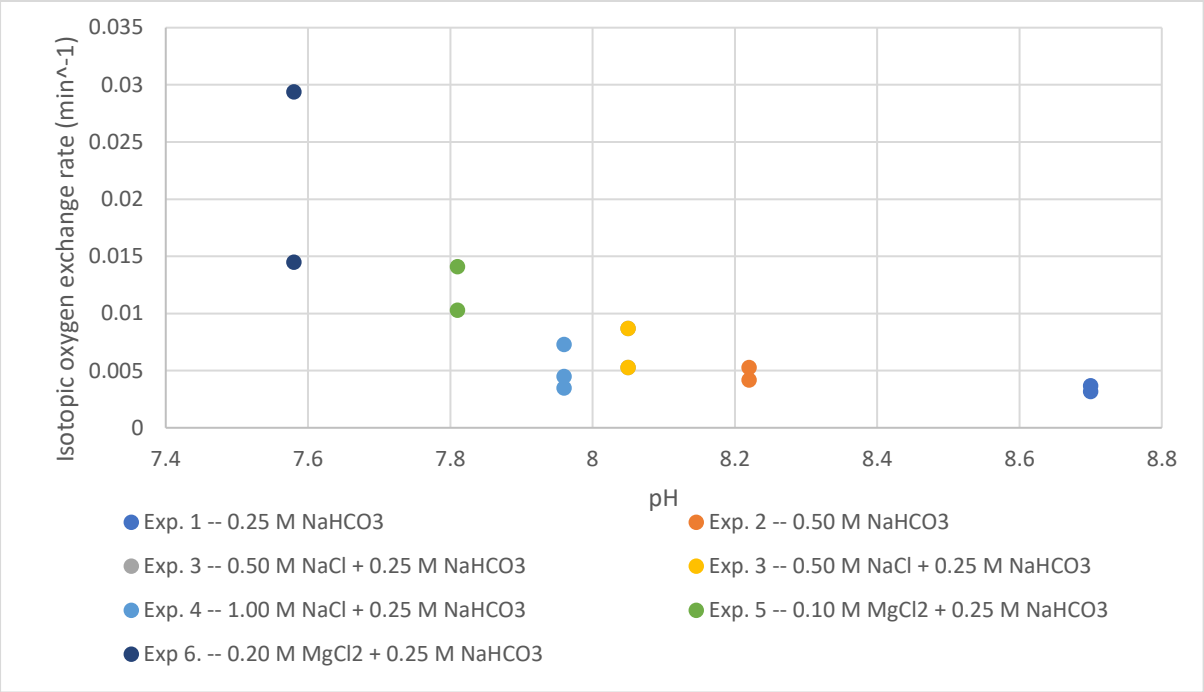

Figure 10: This figure represents the Isotopic oxygen exchange rate vs pH values; each colour represents a duplicate experiment.

3.10 The Full Width Half Maximum.

The Full Width Half Maximum is calculated using the *PsgVoigt1* option in the *fitting tool* of *Witech Control FIVE*. The Full Width Half Maximum represent the width of a peak at half the amplitude. This parameter theoretically could be used to assess the distribution of the ^{18}O over the HCO_3^-(aq) isotopologues. In Table 5 the FHWM are given when the peak of the experiments was located at 1009.0 cm^{-1}, as this shift was found for most experiments, and therefore helped in comparing the experiments at the same point, despite the experiments having different isotopic exchange rates.

Table 5 shows variation in FWHM between the different experiments and duplicate experiments. Whilst duplicate experiments had similar FWHM, like Exp. 4-1 (40.0384 cm^{-1}) and 4-3 (31.2451 cm^{-1}), other experiments had higher variations like Ex. 6-1 (51.0091 cm^{-1}) and Exp.6-2 (45.1312 cm^{-1}). The overall FWHM of the experiments is very large, as Exp. 4-1 had the lowest of 40.04 cm^{-1} and Exp. 2-1 the highest of 52.92 cm^{-1}.

Table 5: The various FWHM at 1009 cm^{-1}, regardless of their timing.

Solution	FWHM at 1009.0 (cm^{-1})		FWHM at 1009.0 (cm^{-1})			
0.25 M NaHCO3	Exp. 1	-	Exp. 1-2	42.3679		
0.50 M NaHCO3	Exp. 2-1	45.4045	Exp. 2-1	52.9243		
0.50 M NaCl + 0.25 M NaHCO3	Exp. 3-1	43.6161	Exp. 3-2	41.9246	FWHM at 1009.0 (cm^{-1})	
1.00 M NaCl + 0.25 M NaHCO3	Exp. 4-1	40.0384	Exp. 4-2	-	Exp. 4-3	41.2351
0.10 M MgCl2+ 0.25 M NaHCO3	Exp. 5-1	45.0592	Exp. 5-2	46.8647		
0.20 M MgCl2+ 0.25 M NaHCO3	Exp. 6-1	51.0091	Exp. 6-2	45.1312		

Discussion

4.1 Identifying the peak at 1367 cm^{-1}.

The peak located around 1367 cm^{-1} (Fig. 5) is found in all the Raman spectra and can correspond to either the v_sCO_2 vibration band of HCO_3^-(aq) (~1364 cm^{-1}) or antisymmetric stretch of C-O of CO_3^{2-} (aq) (~1385 cm^{-1}) (Rudolph et al., 2007). The peak has been identified as the relative activity of the DIC species varies with the pH value of their solution, this relationship is depicted in the Bjerrum plot (Fig. 1). To investigate the peak further, the ~1360 cm^{-1} duplicate peaks of Exp. 1 and Exp. 6 are taken. These were chosen as they had the highest pH value at 8.70, and the lowest pH at 7.58, respectively.

Beginning with HCO_3^-(aq), for which both pH values 8.70 and 7.58 plot near 0 on the Y-axis, indicating that HCO_3^-(aq) is the dominating DIC species. If this was true, all the ~1360 cm^{-1} peaks in Fig. 11 would be displayed at about the same height. In contrast, CO_3^{2-} (aq) peak would have varying heights for the pH values. Exp 1. had a pH value of 8.70 which plots at the Y-axis at log(CO_3^{2-} (aq)/ΣDIC)=-1.8, indicating that CO_3^{2-}(aq) is 0.020 of the total DIC species. Exp. 6 had a pH value of 7.58 plotted at the Y-axis as log(CO_3^{2-}(aq)/ΣDIC)=-2.2, which gives CO_3^{2-}(aq) being 0.006 of the total DIC species. These differences in the activity of CO_3^{2-}(aq) would plot with different heights between the experiments.

The Raman graph (Fig. 11) displays the differences in height of the peaks with the different pH values. The duplicate experiments of Exp. 1 had lower intensity compared to the duplicate peaks of Exp. 6. This evidence suggests that the peak found at ~1360 cm^{-1} is related to the antisymmetric stretch of C-O of CO_3^{2-}.

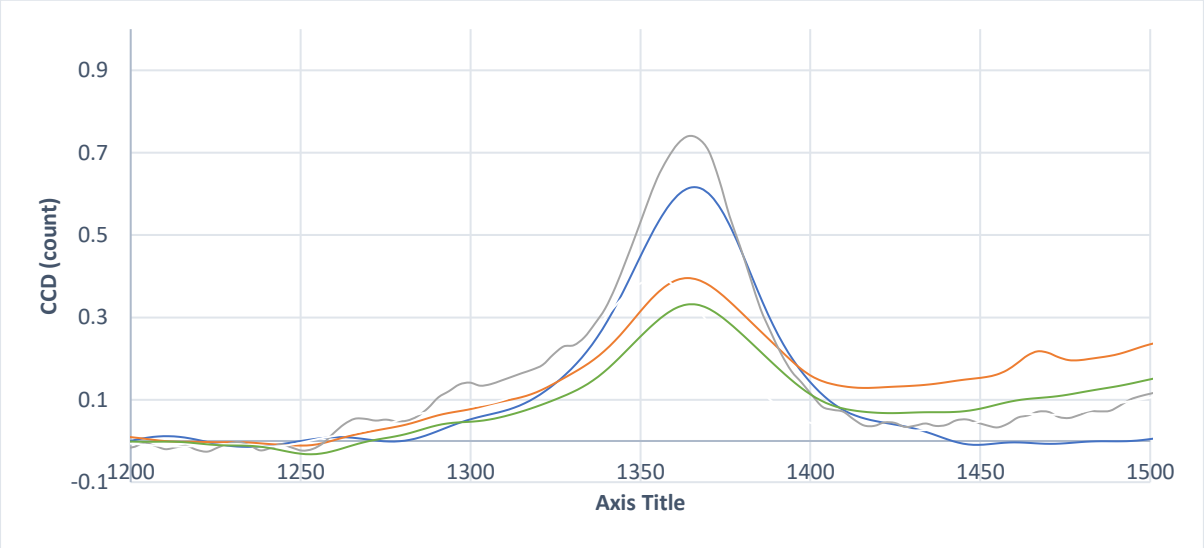

Figure 11: The band at ~1360 cm^{-1}. The y-axis is normalised to the water band at 1640 cm^{-1}. The grey and blue lines represent Exp. 1 (pH 8.70); the green and orange lines represent Exp. 6 (pH 7.58). All data is taken at P=0.

4.2 Contribution of the different isotopologues on the spectra.

Whilst the system is equilibrating to incorporate ^{18}O in the bicarbonate, the peak of the HCO_3^-(aq) band shifts to a lower wavenumber and the width of the band increases as well (Fig. 6). This change in the broadness of a band due to the inclusion of different levels of isotopes have been found in other studies as well, e.g., Weng et al. (2022) observed that a ν_1 band in a carotenoid has the lowest FWHM for either pure ^{12}C or ^{13}C-peak, and the band being the broadest when the ^{13}C and ^{12}C contents are equal. In this study, we have found that the broadening of the band is due to the inclusion of ^{18}O in the four overlapping bands of the HCO_3^-(aq) isotopologues (Fig. 12).

In the case study of Geisler et al. (2012) of CO_3^{2-} the different isotopologues show individual bands which have overlap with each other, but each peak can separately be fitted in a Voigt function. When comparing the bicarbonate band of this study to the carbonate band found in Geisler et al. (2012), we see that the HCO_3^-(aq) is one broadband, whilst the CO_3^-(aq) comprises four individual bands. This indicates that the bicarbonate band is comprised of the four overlapping isotopologues bands instead of the four individual peaks as found for the carbonate isotopologues (Geisler et al. 2012). Although the behaviour in Raman spectroscopy is different, both bicarbonate and carbonate are part of the DIC species and thus are assumed to have largely similar behaviour.

To find the location of the individual bands of the bicarbonate, a model was set up. To model the location of each peak, three main assumptions need to be made.

1) The case that bands formed by different ion pairs and ion conformities without isotopic enrichment are encased within the original $HC^{16}O_3^-$ band. So, when taking the shape and breadth of a new band at a predicted wavenumber, e.g., $HC^{16}O_2{}^{18}O^-$, the same ion pairs or ion structures are found under the new band as they have been found under the original respective $HC^{16}O_3^-$ band. This is done for all the isotopologues.

2) The calculation assumes that the distribution of ^{18}O over the isotopologues of HCO_3^-(aq) and CO_3^{2-}(aq) is the same, thus the different isotopologues having the same isotopic enrichment. The distribution of ^{18}O in CO_3^{-2}(aq) has been estimated based on the relative intensity of the CO_3^{2-}(aq) isotopologues (Jacobs, unpublished). The percentages-wise distribution is applied for these calculations (Table 5).

3) The combination of the different isotopologues' distribution should end up similarly to the equilibrium Raman Spectra (Fig. 10). With these assumptions the following model has been made. The fitting has been done with the free fitting program, Fityk (https://fityk.nieto.pl).

A Voigt fit was made from the natural distribution without any additional ^{18}O incorporation; thus the spectrum was dominated by the $HC^{16}O_3^-$ isotopologue. The area of this band should be about equal to the sum of the areas of all isotopologues together when ^{18}O is added. It is assumed that the ν(C-OH) band can be treated as a harmonic oscillator, so the equation can be used (Geisler et al., 2012):

$$\nu_n = \nu_0 \sqrt{\frac{3m_{16}}{(n \cdot m_{18} + (3-n)m_{16}}}$$

(10)

Where ν_n is the frequency of the n^{th} isotopologues ($HC^{16}O_n{}^{18}O^-_{(n-3)}$), ν_0 is the frequency of $CH^{16}O_3^-$ which is found in an experiment, neglecting very small contributions that may be present from natural ^{18}O

and ^{17}O in the experiment. From this equation, ν_n is found to be 1019 cm^{-1}, and m_{18} and m_{16} are the masses of the isotopes respectively. It is important to note that this equation does not take anharmonic oscillations into account. However, this equation does replicate the carbonate band shifts found for many different solids (King & Živkovi, 2023) and the carbonate ion in the solution.

Table 6: The data used for the different isotopologues. The series refers to the series in Fig. 12, ν is calculated according to (10) and the distributions are taken from Jakobs (unpublished).

Isotopologue	Series	ν (cm^{-1})	Distribution (%)
$HC^{16}O_3^-$	5	1019	25
$HC^{16}O_2{}^{18}O^-$	6	998	41
$HC^{16}O^{18}O_2^-$	7	979	28
$HC^{18}O_3^-$	8	960	6

The percentual distribution that was found in the ^{18}O-isotopologues in $CO^{16}{}_nO^{18}{}_{(3-n)}$ (Jacobs, 2020) is assumed to be equal to the distribution of the ^{18}O in $HCO^{16}O^{18}{}_{(3-n)}^-$. Fytik creates different envelopes for each of the isotopologues, and adding the four envelopes together develops an overall envelope that represents the HCO_3 band in equilibrium. The fit that has formed the peak at 996 cm^{-1}, which agrees with the equilibrated peak ν_{eq} (995.52 cm^{-1}). It is unsure how influential the anharmonic oscillations are on the development of the graph.

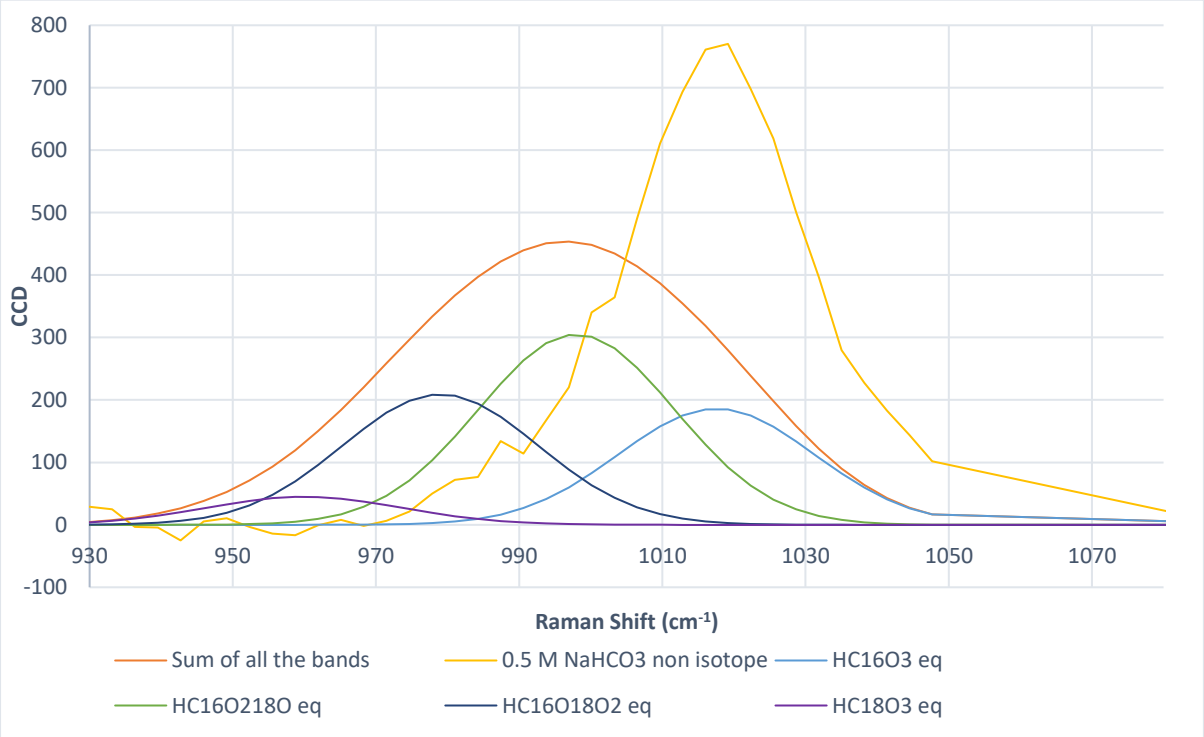

Figure 12: Distribution of the different isotopologue bands after full equilibration. The yellow band is the original non-spiked 0.5 M $NaHCO_3$ band; the orange band is the sum of all the isotopologue bands, and the other bands are the calculated estimates of all the different individual isotopologue peaks.

4.3 The Full Width Half Maximum.

The Full Width Half Maximum (FWHM) of the HCO_3^- bands could provide a way to assess the relative distribution of the different isotopologues underneath the broad envelope, as seen in Figure 12. In the ideal situation, the FWHM should have had the same width over all experiments, as the assumption is made that ^{18}O fractionates linearly over the HCO_3^-. Therefore, when the peak of HCO_3^- (aq) is at a certain shift, it exists at a certain percentage of ^{18}O, and assumptively the distribution of ^{18}O over the isotopologues should be similar under the same conditions.

One of the conditions that have been proven to influence the FWHM of the νC-OH mode of HCO_3^- (aq) is temperature. The study of Rudolph et al. (2007) found that the HCO_3^-(aq) band changed from ~25 cm^{-1} at 20 °C to ~27 cm^{-1} at 50 °C, with a temperature increase of 25 °C and the band only increased 2 cm^{-1}. This factor cannot be the reason for the FHWM being <3 as seen in Table 5.

An explanation yet must be found. It could be that the FWHM is not a good representation of the shape of the data. If the FHWM can connect the distribution of ^{18}O, it can be proven very useful in understanding the effects of ions in the solution and the behaviour of ^{18}O exchange into bicarbonate. At this moment it could not be determined if there is a good correlation, to further investigate this matter, further research should be done in replicating an experiment of one solution and correlating the behaviour of the envelope over time to each other and see if the shape of the envelope is the same after the experiments have reached their isotopic equilibrium.

4.4 Starting position of the HCO_3^- peak.

The x_{in} for the HCO_3^-(aq) peak was observed at 1019.03 cm^{-1} which aligns with (10) and does not fully align with the results found in prior studies that have reported the position of the peak to be either 1017 cm^{-1} (Bonales et al., 2013; Geisler et al., 2012a) or 1016 cm^{-1} (Rudolph et al., 2007). The small changes in shift between the measurements and previous studies can be due to a multitude of factors such as experimental conditions, instrument calibration, and instrument set-up. For instance, the experiments conducted in this study used an incident light of 488 nm, whereas in previous studies a light source of 523 nm was used (Bonales et al., 2013; Geisler et al., 2012a) and the Rudolph et al. (2007) used an incident light of 512 nm.

The peak's location for P=0 for the experiments (shown in Table 7), shows variation and that no experiment corresponded with the location of x_{in}, whilst the experiments were measured under the same conditions with the same equipment. Similar research, using Raman Spectroscopy to trace the ^{18}O substitution from water into DIC species, such as Geisler et al. (2012) and Jakobs (unpublished), have not investigated the starting locations of their experiments, as their research focussed on CO_3^-(aq) which has different bands for each isotopologue, whilst the HCO_3^-(aq) band transforms with changes levels of ^{18}O.

Table 7: All P=0 for all measurements in peak position (cm^{-1}), ordered on similar solutions showing the different experiments. The x_{in} was found at 1019.03 cm^{-1}.

Solution	Peak position P=0 (cm^{-1})		Peak position P=0 (cm^{-1})			
0.25 M NaHCO3	Exp. 1-1	1017.54	Exp. 1-2	1016.98		
0.50 M NaHCO3	Exp. 2-1	1018.54	Exp. 2-2	1017.84		
0.50 M NaCl + 0.25 M NaHCO3	Exp. 3-1	1015.72	Exp. 3-3	1016.60	Peak position P=0 (cm-1)	
1.00 M NaCl + 0.25 M NaHCO3	Exp. 4-1	1014.88	Exp. 4-2	1016.98	Exp. 4-3	1017.02
0.10 M MgCl2+ 0.25 M NaHCO3	Exp. 5-1	1018.81	Exp. 5-2	1017.14		
0.20 M MgCl2+ 0.25 M NaHCO3	Exp. 6-1	1018.50	Exp. 6-2	1015.94		

Some of the difference can be explained by part of the ^{18}O being fractionated into HCO_3^-(aq) between the time of the mixing and P=0 being measured; therefore, some differences are expected between x_{in} and P=0. When having a closer look into the time it took to have the first measurement, it can be separated into two steps. The first step is the time it took the $H_2{}^{18}O$(l) and the solution in the vial to start the first measurement in the Raman Spectrometer. The time of preparation could vary from 0 30 seconds to 2 minutes. The second step is the 5 minutes it took for P=0 to be measured, representing the average of these five minutes. The duration of these two steps is taken as 10 minutes, which is a significant overestimation of the time.

Table 7 shows the variability between the location of P=0, which also means variation between P=0 and x_{in}. For example, the smallest gap between P=0 and x_{in} would be expected at the slowest overall exchange rate of 0.0032 min^{-1}, which was found in Exp 1-1, which had a gap between P=0 and x_{in} of 1.49 cm^{-1}, but the smallest increment was observed in Exp. 5-1 with a gap of 0.23 cm^{-1} which had the third fastest overall oxygen isotopic exchange rate of 0.0141 min^{-1}. These inconsistencies may be due to one or more unattended parameters, such as the influence of temperature on the location of the

HCO_3^-(aq) peak as demonstrated by Rudolph et al. (2007), where the peak shifted from 1016 cm^{-1} at 23 °C to 918 cm^{-1} at 219 °C, as one of the factors for the wide range for the peaks of P=0. It can be suggested that the difference between x_{in} and P=0 cannot be solely explained by oxygen isotope exchange during preparation time. More research into the parameters controlling the oxygen exchange rate should be done, and more replicate experiments of the same solution can lead to a better understanding of the overall behaviour of oxygen isotopic exchange in real time.

4.5 The effects of ionic strength on the isotopic exchange rates.

Figure 9 shows the overall isotopic exchange rate and their ionic strengths, suggesting no clear correlation between ionic strength and the isotopic exchange rate of these experiments. Similar levels of ionic strength can give varying levels of oxygen isotopic exchange rates, whilst similar oxygen exchange rates can have as much as five times the ionic strength. Research conducted by Kim et al. (2014) and Olsen et al. (2022) showed that the effect of NaCl was negligible on the fractionation factors of ^{18}O in the Na-Cl-CO_2-H_2O system. Next to that Uchikawa & Zeebe (2013) showed that Mg^{2+} ions do not have a discernible effect on the oxygen fractionation in the CO_2-H_2O system. It was not possible to detect the isotopic fractionation in Raman Spectroscopy, as was found in Geisler et al. (2012). So, the ionic strength not showing signs of effect on the isotopic exchange rate was not out of line. The effect of the ionic strength on the system could have been confounded by the effects of pH on the oxygen exchange rate. Therefore, research into the effect of ionic strength on the oxygen isotopic exchange rate should be done on a system with equal pH values.

4.6 The effects of pH on the isotopic exchange rates.

Figure 13 shows the effect of pH on the oxygen isotopic exchange rate between $H_2{}^{18}O(l)$ and HCO_3^- (aq) showing an increase in oxygen isotope exchange rate with the decrease of pH value. This trend is not linear, as the isotopic exchange rate increased faster at lower pH values. The change in isotopic exchange rate coincides with the change in the relative activity of the DIC species related to the change in pH of the system (Fig. 1). The pH influences the relative distribution of DIC species affecting the overall oxygen isotopic exchange rate between $H_2{}^{18}O$ and CO_3^{2-}(aq) has been well-documented (Beck et al., 2005; Geisler et al., 2012a; Guo et al., 2019). To test this presumption for HCO_3^-(aq), the measured overall oxygen exchange rates (r) were normalised to the activity of CO_2(aq) (αCO_2(aq)) and the activity of OH^- (αOH^-) to calculate the normalised rates (r') (Geisler et al., 2012).

$$r' = \ln\left(\frac{r}{\alpha_{CO_2} * \alpha_{OH^-}}\right) \quad (11)$$

The values for αCO_2(aq) and αOH^-(aq) were calculated using PHREEQC. Figure 13 shows the results of the normalised pH values, which were around ~14.5 mol^{-1} Ls for all experiments. The fact that the data points plot relatively closely shows that the pH main controlling factor. The variety in the data indicates that there is an unattended parameter outside of pH that has influenced the oxygen isotopic exchange rate.

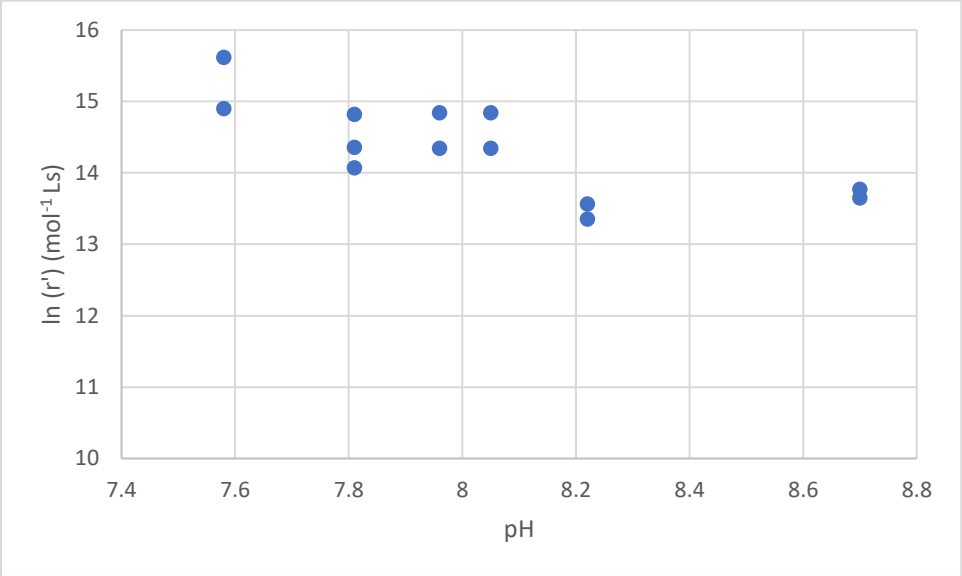

Figure 13: the isotopic exchange rates normalized for the influence vs the pH (r').

The effect of the pH influences the relative distribution of the DIC species as seen in Figure 2 (Beck et al., 2005; Yuen et al., 2016). As the oxygen transfer between H_2O(aq) and HCO_3^-(aq) occurs via hydration (Eq. 2) and hydroxylation (Eq. 3) (Beck et al., 2005; Lueker et al., 2000; Uchikawa et al., 2021), the activity of CO_2(aq) determines the oxygen exchange rate, therefore the oxygen isotopic exchange rates. As the pH value decreased, the oxygen isotopic exchange rate increased logarithmically, which coincides with the logarithmic increase of the activity of CO_2(aq).

4.7 Errors in Preparing the Experiments.

In section 3.7 we have observed that there is a relatively high variation of oxygen isotopic exchange rates between duplicate experiments, during the preparation of the experiments, it is possible that small errors occurred when preparing the bulk solutions. For example, to prepare 10 mL of 0.25 M $NaHCO_3$, an amount of 0.21 g of $NaHCO_3$(s) is required. If this is not done carefully, and for example, an additional 0.01 g $NaHCO_3$ is added, the resulting concentration becomes 0.262 M $NaHCO_3$. Small measuring mistakes can easily lead to variations in the molarities of experiments, which in turn causes differences in the pH and ionic strength of these experiments. Therefore, it is crucial to be cautious and maintain an accurate record of the preparations for the bulk solutions.

As shown in Table 2, Exp. 5 and Exp. 6 produced small traces of precipitate. When determining which experiments were going to be used, a test solution was prepared, which contained a mixture of 0.50 M $NaHCO_3$ and 0.10 $MgCl_2$, which instantaneously produced large amounts of precipitates. To prevent precipitates from forming when mixed with other salts in the solution, a solution of 0.25 M $NaCHO_3$ was used instead of 0.50 M $NaHCO_3$. During the time interval of the experiment, no precipitates were observed, and the solutions remained clear. However, after several days small amounts of precipitate were found in the vials of Exp. 5 and Exp. 6, which may have impacted the oxygen isotope exchange rate.

Another variable that can affect the results is the time between mixing $H_2{}^{18}O$ and the start of the measurement. The oxygen isotopic exchange starts when the ^{18}O-water and the salt solution are mixed. However, before the reaction was measured, the vial needed to be capped, and then put in the path of the incident beam, and the Raman Spectrometer adjusted to the right height to measure the solution. These actions can vary slightly in time, which could be part of the explanation for the different locations of the peaks at P=0, especially in the duplicate experiments, which are elaborated on in section 4.5.

The variation in temperature of the vial may have been affected by the temperature of the hand and the duration of handling and preparing the vial. However, any changes in temperatures would have been limited to the start of the experiments, and the vials would have cooled down to ambient temperature in a matter of minutes. Previous studies have shown that the oxygen isotopic exchange rate increases with temperature as seen (Geisler et al., 2012, Fig. 4) but these studies only considered temperatures between 40 °C to 100 °C with large increments of at least 15 °C. The effects on the isotopic exchange rate around 20 °C with increments in the range of 1 °C are less well researched, thus these temperature changes most likely going to be negligible, as the temperature changes are limited and will be cooled to the surrounding temperature.

Conclusion

In this study we have investigated the ability of Raman Spectroscopy to monitor real-time ^{18}O exchange between $H_2O(l)$ and $HCO_3^-(aq)$ with varying pH and ionic strength, to improve our understanding of the behaviour of oxygen isotopes in DIC species. This has led to the following conclusions:

In this study, we have shown that Raman Spectroscopy can monitor the inclusion of ^{18}O in $HCO_3^-(aq)$ as a decrease in the shift from the natural peak found at 1019 cm^{-1} while the band became broader and lost intensity. This indicated that the band envelope exists of four overlapping bands for each of the isotopologues, each with lower wavenumbers. This change in shift over time was used to determine a way to the ^{18}O exchange rate between $H_2O(l)$ and $HCO_3^-(aq)$.

To determine the location of each band for the isotopologues a model was produced on the assumption that bicarbonate and carbonate show the same behavioural patterns, which fit the measured envelope of equilibrated $HCO_3^-(aq)$ containing 48% ^{18}O.

The broadening of the band was measured using the Full Width Half Maximum, which showed variation between the experiments. This variation did not show usefulness for the FWHM in this study, as no connection could be made between the FWHM and the oxygen isotopic exchange rate.

The effects of different ionic strength on the isotopic exchange rate were shown to be negligible compared to the effect of the pH value of the solution. After the normalisation for pH, the oxygen isotopic exchange rates showed to be similar, suggesting that the pH was the most contributing factor to the oxygen isotopic exchange rate. This was in accordance with pH controlling the activity of the DIC species, determining the activity of $CO_2(aq)$ which determines the exchange of oxygen between $H_2O(l)$ and $HCO_3^-(aq)$ via hydration and hydroxylation.

Altogether, Raman Spectroscopy is a powerful tool for analysing real-time processes on a minute time scale. The analysis of the in-situ exchange of isotopes will help us better understand the kinematics of isotopologues, although unable to detect isotopic fractionation. This knowledge can help us improve our understanding of the impact of different conditions on $^{18}O/^{16}O$, refining our understanding of the $^{18}O/^{16}O$ and thus the climate record.

References

Beck, W. C., Grossman, E. L., & Morse, J. W. (2005). Experimental studies of oxygen isotope fractionation in the carbonic acid system at 15°, 25°, and 40°C. *Geochimica et Cosmochimica Acta*, *69*(14), 3493–3503. https://doi.org/10.1016/j.gca.2005.02.003

Bonales, L. J., Muñoz-Iglesias, V., Santamaría-Pérez, D., Caceres, M., Fernandez-Remolar, D., & Prieto-Ballesteros, O. (2013). Quantitative Raman spectroscopy as a tool to study the kinetics and formation mechanism of carbonates. *Spectrochimica Acta - Part A: Molecular and Biomolecular Spectroscopy*, *116*, 26–30. https://doi.org/10.1016/j.saa.2013.06.121

Cialla-May, D., Schmitt, M., & Popp, J. (2019). Theoretical principles of Raman spectroscopy. *Physical Sciences Reviews*, *4*(6), 1–9. https://doi.org/10.1515/psr-2017-0040

Cui, S., Wang, W., Cheng, C., Yao, Y., Qin, C., & Sun, Q. (2021). Raman quantitative measurement for carbon isotopic composition of CO2: Theory and method. *Chemical Geology*, *585*(September), 120570. https://doi.org/10.1016/j.chemgeo.2021.120570

Das, R. S., & Agrawal, Y. K. (2011). Raman spectroscopy: Recent advancements, techniques and applications. *Vibrational Spectroscopy*, *57*(2), 163–176. https://doi.org/10.1016/j.vibspec.2011.08.003

Devriendt, L. S., Watkins, J. M., & McGregor, H. V. (2017). Oxygen isotope fractionation in the CaCO3-DIC-H2O system. *Geochimica et Cosmochimica Acta*, *214*, 115–142. https://doi.org/10.1016/j.gca.2017.06.022

Gabitov, R. I., Watson, E. B., & Sadekov, A. (2012). Oxygen isotope fractionation between calcite and fluid as a function of growth rate and temperature: An in situ study. *Chemical Geology*, *306–307*, 92–102. https://doi.org/10.1016/j.chemgeo.2012.02.021

Geisler, T., Perdikouri, C., Kasioptas, A., & Dietzel, M. (2012). Real-time monitoring of the overall exchange of oxygen isotopes between aqueous CO 32- and H 2O by Raman spectroscopy. *Geochimica et Cosmochimica Acta*, *90*, 1–11. https://doi.org/10.1016/j.gca.2012.04.058

Guo, Y., Deng, W., & Wei, G. (2019). Kinetic effects during the experimental transition of aragonite to calcite in aqueous solution: Insights from clumped and oxygen isotope signatures. *Geochimica et Cosmochimica Acta*, *248*, 210–230. https://doi.org/10.1016/j.gca.2019.01.012

Kananenka, A. A., & Skinner, J. L. (2018). Fermi resonance in OH-stretch vibrational spectroscopy of liquid water and the water hexamer. *Journal of Chemical Physics*, *148*(24). https://doi.org/10.1063/1.5037113

Kim, S. T., Gebbinck, C. K., Mucci, A., & Coplen, T. B. (2014). Oxygen isotope systematics in the aragonite-CO2-H2O-NaCl system up to 0.7mol/kg ionic strength at 25°C. *Geochimica et Cosmochimica Acta*, *137*, 147–158. https://doi.org/10.1016/j.gca.2014.02.050

Kim, S. T., O'Neil, J. R., Hillaire-Marcel, C., & Mucci, A. (2007). Oxygen isotope fractionation between synthetic aragonite and water: Influence of temperature and Mg2+ concentration. *Geochimica et Cosmochimica Acta*, *71*(19), 4704–4715. https://doi.org/10.1016/j.gca.2007.04.019

King, H. E., & Geisler, T. (2018a). Tracing mineral reactions using confocal raman spectroscopy. In *Minerals* (Vol. 8, Issue 4). MDPI AG. https://doi.org/10.3390/min8040158

King, H. E., Plümper, O., Geisler, T., & Putnis, A. (2011). Experimental investigations into the silicification of olivine: Implications for the reaction mechanism and acid neutralization. *American Mineralogist*, *96*(10), 1503–1511. https://doi.org/10.2138/am.2011.3779

King, H. E., & Živkovi, A. (2023). *Evaluating the Effect of 18 O Incorporation on the Vibrational Spectra of Vaterite and Calcite*. https://doi.org/10.3390/cryst13010048

Lueker, T. J., Dickson, A. G., & Keeling, C. D. (2000). Ocean p CO 2 calculated from dissolved inorganic carbon , alkalinity , and equations for K 1 and K 2 : validation based on laboratory measurements of CO 2 in gas and seawater at equilibrium. *Marine Chemistry*, *70*, 105–119.

Olsen, E. K., Watkins, J. M., & Devriendt, L. S. (2022). Oxygen isotopes of calcite precipitated at high ionic strength: CaCO3-DIC fractionation and carbonic anhydrase inhibition. *Geochimica et Cosmochimica Acta*, *325*, 170–186. https://doi.org/10.1016/j.gca.2022.01.028

O'Neil, J. R., Vennemann, T. W., & McKenzie, W. F. (2003). Effects of speciation on equilibrium fractionations and rates of oxygen isotope exchange between (PO4)aq and H2O. *Geochimica et Cosmochimica Acta*, *67*(17), 3135–3144. https://doi.org/10.1016/S0016-7037(02)00970-5

Rudolph, W. W., Irmer, G., & Königsberger, E. (2007a). Speciation studies in aqueous HCO3−–CO32− solutions. A combined Raman spectroscopic and thermodynamic study. *Journal of the Chemical Society. Dalton Transactions*, *3*(7), 900–908. https://doi.org/10.1039/b713254a

Rudolph, W. W., Irmer, G., & Königsberger, E. (2007b). Speciation studies in aqueous HCO3−–CO32− solutions. A combined Raman spectroscopic and thermodynamic study. *Journal of the Chemical Society. Dalton Transactions*, *7*, 900–908. https://doi.org/10.1039/b713254a

Tarutani, T., Clayton, R. N., & Mayeda, T. K. (1969). The effect of polymorphism and magnesium substitution on oxygen isotope fractionation between calcium carbonate and water. *Geochimica et Cosmochimica Acta*, *33*(8), 987–996. https://doi.org/10.1016/0016-7037(69)90108-2

Uchikawa, J., Chen, S., Eiler, J. M., Adkins, J. F., & Zeebe, R. E. (2021). Trajectory and timescale of oxygen and clumped isotope equilibration in the dissolved carbonate system under normal and enzymatically-catalyzed conditions at 25 °C. *Geochimica et Cosmochimica Acta*, *314*, 313–333. https://doi.org/10.1016/j.gca.2021.08.014

Uchikawa, J., & Zeebe, R. E. (2012). The effect of carbonic anhydrase on the kinetics and equilibrium of the oxygen isotope exchange in the CO 2-H 2O system: Implications for δ 18O vital effects in biogenic carbonates. *Geochimica et Cosmochimica Acta*, *95*, 15–34. https://doi.org/10.1016/j.gca.2012.07.022

Uchikawa, J., & Zeebe, R. E. (2013). No discernible effect of Mg2+ ions on the equilibrium oxygen isotope fractionation in the CO2-H2O system. *Chemical Geology*, *343*, 1–11. https://doi.org/10.1016/j.chemgeo.2013.02.002

Weckhuysen, B. M., & Wachs, I. E. (1997). In Situ Raman Spectroscopy of Supported Chromium Oxide Catalysts: 18 O 2 − 16 O 2 Isotopic Labeling Studies . *The Journal of Physical Chemistry B*, *101*(15), 2793–2796. https://doi.org/10.1021/jp963101l

Weng, J., Müller, K., Morgaienko, O., Elsner, M., & Ivleva, N. P. (2022). Multi-element stable isotope Raman microspectroscopy of bacterial carotenoids unravels rare signal shift patterns and single-cell phenotypic heterogeneity. *Analyst*, 128–136. https://doi.org/10.1039/d2an01603f

Wiley, J., & Edwards, H. G. M. (2005). Book Review Modern Raman Spectroscopy-A Practical Approach Ewen Smith and Geoffrey Dent. *JOURNAL OF RAMAN SPECTROSCOPY J. Raman Spectrosc*, *36*, 835. https://doi.org/10.1002/jrs.1320

Yuen, Y. T., Sharratt, P. N., & Jie, B. (2016). Carbon dioxide mineralization process design and evaluation: concepts, case studies, and considerations. *Environmental Science and Pollution Research*, *23*(22), 22309–22330. https://doi.org/10.1007/S11356-016-6512-9

Zeebe, R. E. (2001). Seawater pH and isotopic paleotemperatures of Cretaceous oceans. *Palaeogeography, Palaeoclimatology, Palaeoecology*, *170*(1–2), 49–57. https://doi.org/10.1016/S0031-0182(01)00226-7

Zeebe, R. E., & Wolf-Gladrow, D. (2001). *CO2 in Seawater: Equilibrium, Kinetics, Isotopes* (1st ed.). Elsevier Ltd.